Int. J. Electrochem. Sci., 14 **(2019)** 1763 – 1772, doi: 10.20964/2019.02.45

International Journal of
ELECTROCHEMICAL
SCIENCE
www.electrochemsci.org

Reduced Graphene Oxide Wrapped Sulfur/Polypyrrole Composite Cathode with Enhanced Cycling and Rate Performance for Lithium/Sulfur Batteries

Guanghui Yuan[1*], *Huafeng Jin*[1], *Yan Zhao*[2*]

[1] School of Chemistry and Chemical Engineering, Research Centre of New Materials, Ankang Research Centre of Zn Based Materials Science and Technology, Ankang University, Shaanxi Ankang, China
[2] Synergy Innovation Institute of GDUT, Heyuan, Guangdong Province, China
[*]E-mail: chem_yuan@163.com; zhaoyan_sii@163.com

Received: 24 August 2018 / *Accepted:* 19 November 2018 / *Published:* 5 January 2019

An innovative reduced graphene oxide wrapped sulfur/polypyrrole (S/PPy@RGO) composite is synthesized via a one-pot polymerization of pyrrole monomer in a sulfur/reduced graphene oxide aqueous suspension. This one-pot preparation method is efficient through its inherent simplicity and low cost. The resultant S/PPy@RGO composite was characterized via EDS, XRD, SEM, TEM and electrochemical measurements. In the S/PPy@RGO ternary composite, reduced graphene oxide played a crucial role of coating a thin layer to trap soluble polysulfide intermediates, provide a continuous electrically conducting network and accommodate volume expansion. Meanwhile polypyrrole with its high absorptivity, joins sulfur and RGO as a binding agent, and tether polysulfides into its porous framework. Therefore, the synthesized S/PPy@RGO composite delivers excellent rate ability and highly cycling stability. This composite can retain a specific discharge capacity of 615.3 mAh g^{-1} at 0.2C, even after 100 cycles.

Keywords: S/PPy@RGO composite; one pot polymerization; lithium/sulfur batteries; electrochemical performance

1. INTRODUCTION

Rechargeable lithium-ion batteries have maintained dominance in the energy storage industry for portable devices encompassing primarily of cellphones, laptops, and cameras. However, use of this technology in electricand hybrid vehicles, and large-scale grid energy storage systems still necessitates the evolution of the rate performance and cathode capacity [1,2]. Elemental sulfur (S) has led an opportune impetus in the development of novel cathode materials for next-generation, secondary lithium

batteries exploiting its abundant availability, environmental benignity, low cost, and theoretical specific energy of 2600 Wh kg^{-1} and theoretical capacity of 1672 mAh g^{-1} [3,4].

Albeit the promising attributes, Lithium/Sulfur (Li/S) batteries are typically hindered by its inherently low material-utilization and poor cycle stability. These setbacks arise from sulfur's low electron conductivity and irreversible polysulfide formation in the organic electrolyte [5,6]. In response, considerable research has been directed at surmounting the insulating nature of the S cathode, not withholding the development of numerous sulfur/conductive carbon [7-9] and sulfur/conductive polymer composites [10-13]. In particular, combinations of sulfur and PPy have been thoroughly perused due to PPy's strong absorptivity, which can mitigate polysulfide dissolution [11-13]. However, further advancement of this technology is still bottle-necked by the low electronic conductivity of the S/PPy composite. Additionally, the sulfur on the surface is vulnerable to the electrolyte and the polysulfides, which develops during the cell discharge, and easily diffuses into the electrolyte. Two-dimensional graphene is the go-to substrate for Li/S batteries due to its excellent conductivity, immense surface area for active material deposition, and elasticity to accommodate volume changes [3,14]. Most recently, reduced graphene oxide has attracted great attention because a thin layer can be coated on the surface of sulfur particles to withhold the diffusion of polysulfides, favoring an enhanced electrochemical performance [15-19].

Herein, we describe the preparation of a novel reduced graphene oxide wrapped sulfur/polypyrrole (S/PPy@RGO) composite via a one-pot polymerization of the pyrrole monomer amidst a nano-sulfur and reduced graphene oxide solution. Furthermore, as a cathode for secondary lithium batteries, the physical and electrochemical properties of the resultant composite are also presented.

2. EXPERIMENTAL

Graphite oxide (GO) was synthesized via modified Hummers method, as described elsewhere [20]. In a typical method, 0.800 g natural graphite (Alfa Aesar) was mixed into 23.0 mL concentrated H_2SO_4 (98%) and stirred in an ice bath for 24 h. 3.000 g $KMnO_4$ (Sigma-Aldrich) was afterwards mixed into the solution while the temperature was kept below 20 °C. Subsequently, the mixture was diluted and heated up to 100 °C for 15 min. Furthermore, the reaction was eliminated by adding 10.0 mL concentrated H_2O_2 (30%) and 140.0 mL deionized (DI) water. Finally, the ensuing GO suspension was thoroughly rinsed with 5 % HCl solution and DI water until the solution reached a pH of 7. For reducing, 0.100 g GO was dispersed into 50.0 mL DI water, 1 mL hydrazine monohydrate (Sigma-Aldrich) was subsequently added to the mixture and heated at 95 °C for 12 h. Next, the RGO was filtrated and collected as a black powder. Finally, the product was rinsed several times with DI water to remove any excess hydrazine, and left to dry at 75 °C overnight in a vacuum oven.

Polypyrrole via the chemical oxidative procedure [21], was prepared by mixing the pyrrole monomer (Aldrich, 98% purity) with the oxidiant, $FeCl_3$ (Sigma-Aldrich, 97%). 0.005 g RGO was first dispersed in 40.0 mL DI water at room temperature for 2 h using an ultrasonic homogenizer (Fisher Scientific, FB120). 3.000 g nano-sulfur aqueous suspension (US research nanomaterials Inc, 10 wt%)

was slowly incorporated into the RGO suspension and magnetically stirred for 3 h. Afterwards, 0.100 g pyrrole was added into the mixture and stirred for 0.5 h before dropwise adding 10.0 mL of a 0.5 mol L^{-1} $FeCl_3$ solution under sonication. Moreover, the solution was further sonicated for another 2 h. Centrifugation was used to separate and collect the precipitate of S/PPy@RGO, followed by repeated DI water washing, and then dried overnight in a vacuum oven at 75 °C to yield the S/PPy@RGO composite. For comparison, sulfur/polypyrrole (S/PPy) composites without the addition of RGO was also prepared for electrochemical testing.

X-ray diffraction (XRD, D8 Discover, Bruker) equipped with Cu Kα radiation was used to investigate the crystalline phase of the samples. The thickness and morphology of the sample was investigated using a Pico Scan atomic force microscope (AFM, Molecular Imaging, Bruker). Raman (RAM, HR300, Jobin-Yvon) was evaluated with a Raman spectrometer equipped with a 532 nm green laser source. The morphology of the composite surface was screened by a field-emission scanning electron microscopy (FE-SEM, Leo-1530, Zeiss). The internal framework was inspected with a high-resolution transmission electron microscopy (HRTEM, TITAN 80-300, FEI) set up with an Energy Dispersive Spectroscopy (EDS). The sulfur content in the S/PPy@RGOand S/PPy composites were determined as 63.0% and 62.5% using chemical analysis (CHNS, Vario Micro Cube, Elementar).

The electrochemical performance of S/PPy@RGO and S/PPy composites were investigated within coin-type cells (CR2032). The cells were comprised of a S/PPy@RGO (or S/PPy) cathode, a lithium metal anode, and a polypropylene separator immersed in 1.0 mol L^{-1} lithium bistrifluoromethanesulfonamide (LiTFSI) (Aldrich, 96% purity) in tetraethylene glycol dimethyl ether (TEGDME) (Aldrich, 99% purity) electrolyte. More specifically, the composite cathodes were prepared by blending in 1-methyl-2-pyrrolidinone (NMP, Sigma-Aldrich, ≥99.5% purity): 80 wt% S/PPy@RGO or S/PPy composite, 10 wt% polyvinylidene fluoride (PVdF) (Kynar, HSV900) as a binder, and 10 wt% acetylene black (MTI, 99.5% purity) as a conducting agent . The resulting slurry was coated onto Al foil and vacuum-dried overnight at 60 °C. The coin cells were assembled in argon-filled (99.9995 % purity) Braun glovebox. The cells were evaluated between 1.5 and 3.0 V vs. Li^+/Li electrode on a multichannel battery tester (BT-2000, Arbin Instruments). Specific capacities and applied currents were evaluated on a weight basis with respect to the S in the cathode.

3. RESULTS AND DISCUSSION

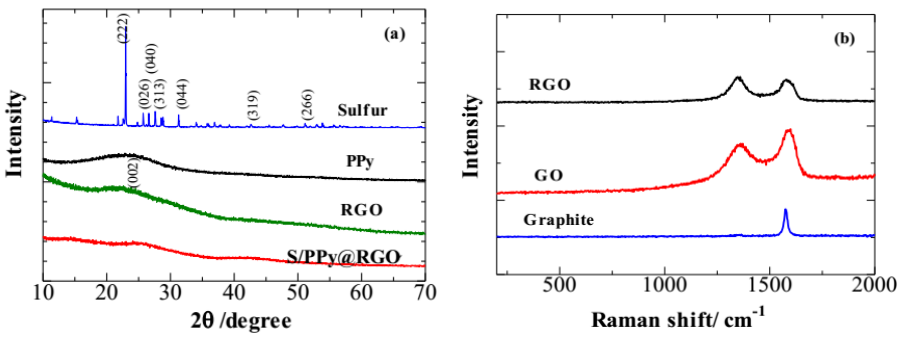

Figure 1. (a) XRD spectra of sulfur, PPy, RGO and S/PPy@RGO composite. (b) Raman spectra of graphite, GO and RGO.

Fig.1a displays the XRD spectra of PPy, RGO, S and S/PPy@RGO composite samples. The pattern corresponding to PPy exhibits a wide diffraction peak at 25.0° as a result of pyrrole intermolecular packing [22]. A weak RGO (002) peak is observed at 23.5°, confirming that RGO was successfully prepared upon the reduction of GO as reported in our previous work [15]. Because of the low RGO content and its well-dispersion, the reflection of RGO at 23.5° is hardly detected for the S/PPy@RGO composite. The S used in this work exhibits obvious peaks at about 23.2°, 25.9°, 27.7°, 28.8°, 31.6°, 42.9°, and 51.4° indexing to (222), (026), (040), (313), (044), (319) and (266) planes of the *Fddd* orthorhombic structure for elemental sulfur (JCPDS #08-0247). However, these sharp peaks disappear in the S/PPy@RGO composite spectra. This is most probable by cause of the well-dispersed nature of nanoscopic sulfur in the composite, as evidenced by the following EDS analysis. Moreover in Fig. 1b, Raman spectroscopy was employed to characterize the pristine graphite, GO and RGO. The presence of pristine graphite was confirmed by the prominent G band located at 1581 cm^{-1} and a negligible D band at 1361 cm^{-1}. However in the spectra of GO, the G band broadens while the D band expands, corresponding to the enlarging of sp^3 domains. Contrasting RGO to GO, the increased D/G-band ratio can be attributed to the formation of new graphitic domains and the average size contraction of sp^2 domains [23].

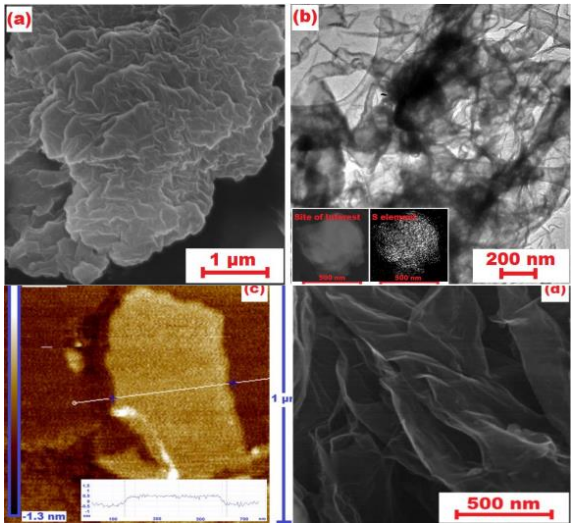

Figure 2. (a) SEM image of S/PPy@RGO composite. (b) TEM image of S/PPy@RGO composite. Inset contains an EDS map of the sulfur distribution in the S/PPy@RGO composite. (c) AFM image of RGO sheets with a linear height profile, as denoted by the white line. (d) SEM image of highly wrinkled RGO.

The surface morphology of the S/PPy@RGO composite imaged by SEM is depicted in Fig. 2a. The S/PPy@RGO composite demonstrates a typical curved, layer-like structure; the S/PPy particles are well-wrapped within many RGO layers. Furthermore, the surface appears to be wrinkled in the S/PPy@RGO composite. The HRTEM in Fig. 2b confirms the S/PPy particles have been coated within graphene layers, i.e. a flexible and corrugated thin-film of graphene and a dense S/PPy core are readily observed. The EDS mapping (inset of Fig. 2b) affirms the highly homogeneous dispersion of nanoscopic sulfur in the S/PPy@RGO composite. Moreover, AFM quantified the thickness and displayed the

morphology of these RGO sheets in the S/PPy@RGO composite. An RGO sheet was casted on a silicon wafer and investigated by tapping-mode AFM. Moreover, fig. 2c shows a 1 nm thick RGO sheet, entailing the successful exfoliation of graphite. The morphology and microstructure of the resultant RGO was characterized by SEM as shown in Fig. 2d. More specifically, the graphene nanosheets possessed an ultrathin thickness with a highly wrinkled surface consistent with the former AFM observation.

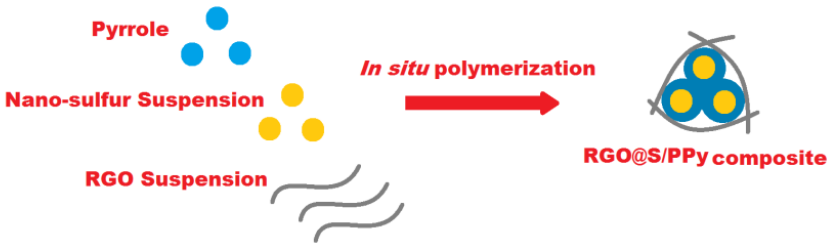

Figure 3. Schematic of the synthesis process of S/PPy@RGO composite.

Upon consolidating the gathered data, a potential process of formation for the composite is suggested in Fig. 3. Corresponding to the proposed scheme, pyrrole is firstly polymerized in the presence of RGO and sulfur. Since freshly polymerized PPy has a strong affinity toward sulfur and RGO, PPY will benefit as a tether for both the sulfur nanoparticles and RGO. Meanwhile, the RGO wraps around the S/PPy particles, serving as both a conducting substrate for the otherwise insulating sulfur and a barrier to impede polysulfide dissolution.

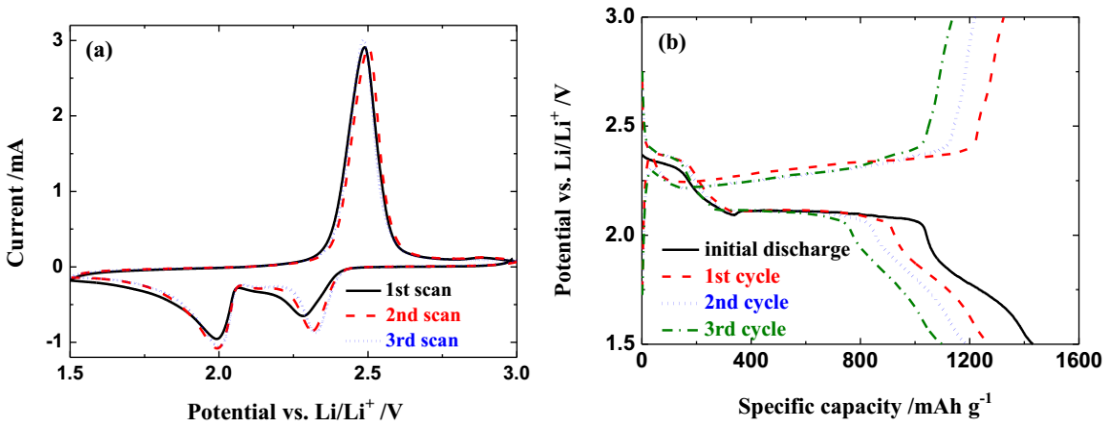

Figure 4. The (a) first three CV cycles of the S/PPy@RGO composite electrode at a scan rate of 0.15 mV s^{-1} between 1.5 and 3.0 V, and (b) first three charge–discharge cycles of the S/PPy@RGO composite electrode at 0.1 C.

To study the effect of RGO and PPy in promoting electrochemical properities, many electrochemical measurements were recorded and discussed. The CV curves of S/PPy@RGO composite cathode were tested in Li/S batteries in the range of 1.5~3.0 V at 0.1 mV s^{-1}, as illustrated in Fig. 4a. It apparent that all the three CV curves reveal the typical characteristic peaks at about 2.0 V and 2.3 V. The cathodic peak at around 2.3 V can be associated to the reduction of S to Li_2S_n (n ≥4). The other cathodic peak at 2.0 V corresponds to the reduction of Li_2S_n into Li_2S_2 and Li_2S [24]. In each of the three

anodic scans, only one strong characteristic peak is detected at about 2.5 V, which can be assigned to the oxidation of Li_2S and Li_2S_2 to Li_2S_8 [25]. During the first three cycles, all the redox peak potentials and currents exhibit great repeatability, demonstrating excellent reversibility and stability of the S/PPy@RGO electrode. Additionally, Fig. 4b shows the first three charge-discharge cycles of the S/PPy@RGO electrode at a current density of 0.1 C (1 C = 1670 mAh g^{-1}). Specifically, the S/PPy@RGO electrode exhibits two unmistakable plateaus, at around 2.0 V and 2.3 V, in a discharge cycle and one apparent plateau at about 2.4 V in the charge cycle. Thus, the plateau potentials of the charge-discharge curves are in accord with data derived from the CV curves. In the initial discharge process at 0.1 C, the S/PPy@RGO electrode exhibitsx the highest discharge capacity of 1431.7 mAh g^{-1}. After 3 cycles at 0.1 C, the S/PPy@RGO electrode exhibits a charge capacity of 1139.0 mAh g^{-1}, a complementary discharge capacity of 1099.2 mAh g^{-1}, and a high coulombic efficiency of 96.5%.

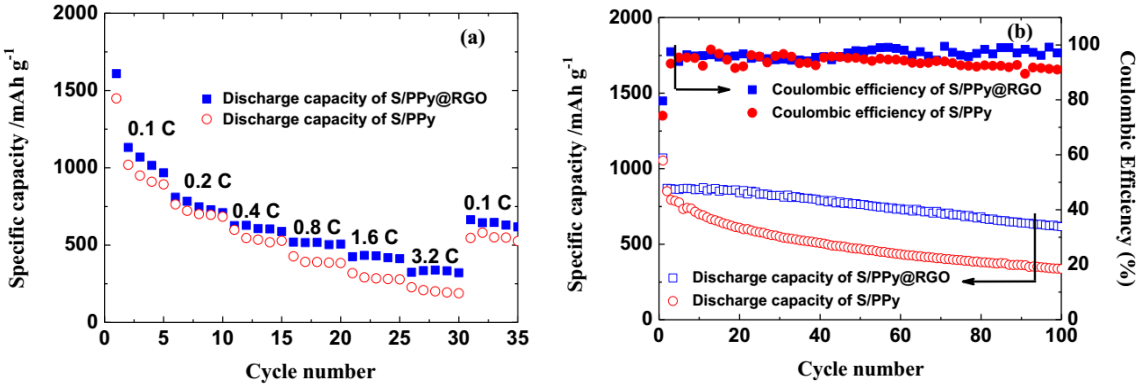

Figure 5. (a) Rate performance and (b) cycle performance of the S/PPy@RGO and S/PPy electrodes at 0.2 C.

The current rate ability and cycle performance of electrodes are two very crucial, yet lacking characteristics for Li/S battery applications. For comparison, S/PPy composite is chosen as cathode in Li/S batteries during the cells testing. The rate abilities of S/PPy and S/PPy@RGO electrodes are firstly investigated at different charge-discharge rates, as demonstrated in Fig. 5a. Predictably, the reversible discharge capacities of both S/PPy and S/PPy@RGO electrodes decrease regularly with the increased rate. This can be explained by increasing the current density, less and less active sulfur participate in the electrochemical reactions. As an example, the reversible discharge capacities of 1131.2, 809.1, 625.9, 519.1, 424.9 and 323.6 mAh g^{-1} of the S/PPy@RGO electrode were recorded at 0.1 C, 0.2 C, 0.4 C, 0.8 C, 1.6 C and 3.2 C, respectively. However, decreasing the current to 0.1 C rate practically recovered the reversible discharge capacity back to 664.3 mAh g^{-1}. Comparing to the S/PPy electrode, the S/PPy@RGO electrode has a greater reversible discharge capacity of 20~100 mAh g^{-1} at each current density. In detail, the reversible discharge capacities of 1019.1, 763.3, 598.5, 427.2, 318.0 and 227.0 mAh g^{-1} of the S/PPy electrode are obtained at 0.1 C, 0.2 C, 0.4 C, 0.8 C, 1.6 C and 3.2 C, respectively. However, when the current is cycled back to 0.1 C rate, a mere reversible discharge capacity of 545.4 mAh g^{-1} was obtained. The rate ability of the S/PPy@RGO electrode is clearly superior to that of the S/PPy electrode, especially at higher charge/discharge rates.

The 0.2 C cycling performance of the S/PPy and S/PPy@RGO electrodes are shown in Fig. 5b. The Li/S battery equipped with a S/PPy@RGO electrode can exhibit an initial specific discharge capacity of 1070.5 mAh g^{-1} and a reversible capacity of 869.6 mAh g^{-1}. After 100 cycles at 0.2 C, the specific discharge capacity of the S/PPy@RGO electrode maintained a high 615.3 mAh g^{-1}, exhibiting excellent cycle stability. The coulombic efficiency steadily reached around 98% after several cycles. Contrastingly, the Li/S battery with S/PPy electrode can deliver an initial specific discharge capacity of 1054.3 mAh $g^{-1}$and a subsequent reversible capacity of 851.1 mAh g^{-1}. Albeit the two electrodes have similar capacities after a few cycles, the ensuing discharge capacities of S/PPy electrode fades dramatically upon further cycling. After 100 cycles at 0.2 C, the S/PPy electrode can only deliver 335.4 mAh g^{-1}, which is roughly half of the specific discharge capacity of the S/PPy@RGO electrode. Moreover, the coulombic efficiency of the S/PPy electrode gradually drops to around 95% after 100 cycles. It is noticeable that the S/PPy@RGO electrode exhibits a superior cycling stability than that of the S/PPy electrode. The enhanced rate ability and cycle performance of S/PPy@RGO composite can be contributed to the synergistic effects between RGO and PPy. In the S/PPy@RGO ternary composite, PPy acts not only as a fence to accustom the sulfur volume expansion, but also as a binder to join sulfur and RGO. As well, the S/PPy particles were homogenously dispersed over the cross-linked RGO nanosheets, which shortened the Li^+ diffusion avenues and provided accelerated ion-transport pathways. Besides providing a conducting coating layer, the RGO plays a role of an active absorber to trap soluble polysulfide intermediates.

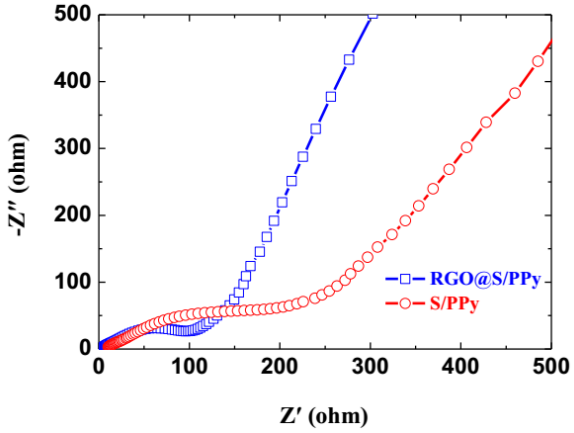

Figure 6. Nyquist plots of S/PPy@RGO and S/PPy electrodes scanned between 100 kHz to 0.01 Hz.

To elaborate on the effects of RGO on the conductivity and charge transfer behavior in the S/PPy@RGO ternary composite, comparative EIS measurements for the S/PPy@RGO and S/PPy composites were conducted after the first charge-discharge process. Thus, the EIS data is presented in Fig. 6. Firstly, both impedance plots are similar, displaying the typical semicircle at the higher frequency region and the typical slanted, straight line in the lower frequency range. To elaborate, the semicircle corresponds to the charge transfer resistance of the composite cathode, while the straight line represents the Li^+ diffusion from the electrodes into the active materials [26-28]. As extrapolated from Fig. 6, the charge transfer resistance of the S/PPy@RGO cathode is 96.0 Ω, which is superior than that of the S/PPy

cathode (203.9 Ω). The results conclude that the RGO additive can definitely enhance the conductivity of the composite. Furthermore, the straight line in the EIS data of S/PPy@RGO cathode displays more slope than that of the S/PPy cathode, illustrating that S/PPy@RGO composite can provide quicker ion transport pathways than the S/PPy composite. Moreover, the EIS data also confirmed that the electrochemical reaction activity of the electrode has been conclusively bettered with the incoporation of RGO, which support our previous suggestions on the conductivity improvement of the S/PPy@RGO composite.

Reflecting on the detailed electrochemical investigations of the S/PPy@RGO composite, the as-prepared ternary material exhibited good reversible capacity and capacity retention in contrast to the current research, as listed in Table 1. The electrochemical characteristics, in pertaining to the reversible lithium intercalation, are remarkable when considering that our proposed sample is synthesized by one-pot polymerization, which possesses many advantages including simplicity and low cost. It is worth mentioning that in comparison with the theoretical capacity of sulfur, the S/PPy@RGO electrode is not yet adequate in lithium storage capacity. Recent works have also reported that metal oxides can establish relatively strong chemical bonds with polysulfides to contain the polysulfides, which can also improve the lithium storage capacity in sulfur electrodes [30,34-36]. Therefore, supplementing metal oxides into our work may further enhance its electrochemical performance.

Table 1. Table to compare electrochemical performances of S−based cathodes in Li/S batteries.

Sample	Reversible capacity (mAh g^{-1})	Cycle number	Capacity retention	Potential (V vs. Li^+/Li)	Current density	Ref
S/PPy@RGO	1071	100th	57.9%	1.5−3.0 V	0.2 C	this work
S/GN	892	80th	43.7%	1.0−3.0 V	0.2 C	[7]
S/GO	1069	100th	37.9%	1.0−3.0 V	0.1 C	[14]
S/T-PPy	1152	80th	56.4%	1.0−3.0 V	0.1 C	[29]
HCF/S	1205	40th	34.0%	1.7−2.8 V	0.2 C	[30]
MnO_2@HCF/S	1147	100th	77.6%	1.7−2.8 V	0.2 C	[30]
S/MWCNT	1063	50th	65.5%	1.0−3.0 V	0.1 C	[31]
GSH-S	950	100th	55.3%	1.5−3.0 V	1.0 C	[32]
rGO-S	1020	100th	57.1%	1.5−3.0 V	0.2 C	[33]

4. CONCLUSIONS

A novel reduced graphene oxide wrapped sulfur/polypyrrole (S/PPy@RGO) composite was successfully prepared *via a* one-pot polymerization of pyrrole monomer in the presence of nano-sulfur and reduced graphene oxide (RGO) aqueous suspension, and subsequent heat-treatment. The collective effects of RGO and polypyrrole (PPy) were the key factors to the superb high discharge rate performance of the sulfur composite cathode. Namely, the RGO coating layer plays a crucial role in providing both a suitable lithium ion transport path and a retardation towards the diffusion of polysulfides into the

electrolyte. Meanwhile, polypyrrole with its high absorption capabilities, act as a binder to join sulfur and RGO and bind the polysulfides to its absorptive framework. Lastly, the S/PPy@RGO composite cathode manifested excellent cycling stability and much potential for the advancement of secondary sulfur/lithium batteries.

ACKNOWLEDGMENTS
The authors would like to express their gratitude for the financial support provided by the Natural Science Fund of Education Department of Shaanxi Provincial Government (Grant No. 15JK1004), and the Subject Merging Fund and the Natural Science Fund from Ankang University for high-level talents (Grant Nos. 2016AYQDZR05 and 2017AYJC01).

AUTHOR CONTRIBUTIONS
G. Y. was responsible for conceiving and designing the experiments, while H. Ji. conducted the experimental procedure and evaluated the resulting data. All authors contributed in preparing the draft and revisions of the manuscript. Lastly, Y. Z. and G. Y. oversaw the endeavor and consummated the manuscript. All authors read and commented on the manuscript.

CONFLICTS OF INTEREST
The authors declare no conflict of interest.

References

1. S. Evers and L.F. Nazar, *Acc. Chem. Res.*, 46 (2013) 1135.
2. A. Marongiu, M. Roscher and D.U. Sauer, *Appl. Energ.*, 137 (2015) 899.
3. S. Li, Z. Luo, X. Cao, G. Fang and S Liang, *Int. J. Electrochem. Sci.*, 13 (2018) 23.
4. Y.G. Zhang, L.C. Sun, H.P. Li, T.Z. Tan and J.D. Li, *J. Alloy. Compd.*, 739 (2018) 290.
5. S.H. Chung, C.H. Chang and A. Manthiram, *Energ. Environ. Sci.*, 9 (2016) 3188.
6. A. Rosenman, E. Markevich, G. Salitra, D. Aurbach, A. Garsuch and F.F. Chesneau, *Adv. Energ. Mater.*, 5 (2015) 1500212.
7. G. Yuan, G. Wang, H. Wang and J. Bai, *J. NanoPart. Res.*, 17 (2015) 36.
8. T. Gao, T. Le, Y. Yang, Z. Yu, Z. Huang and F. Kang, *Materials*, 10 (2017) 376.
9. J.H. Kim, K. Fu, J. Choi, S. Sun, J. Kim, L. Hu and U. Paik, *Chem. Commu.*, 51 (2015) 13682.
10. X. Liang, M. Zhang, M.R. Kaiser, X. Gao, K. Konstantinov, R. Tandiono and J. Wang, *Nano Energ.*, 11 (2015) 587.
11. Y. Xie, H. Zhao, H. Cheng, C. Hu, W. Fang, J. Fang and Z. Chen, *Appl. Energ.*, 175 (2016) 522.
12. Y.G. Zhang, Y. Zhao, Z. Bakenov, M. Tuiyebayeva, A. Konarov and P. Chen, *Electrochimica Acta.*, 143 (2014) 49.
13. F.X. Yin, X.Y. Liu, Y.G. Zhang and Y. Zhao, *Solid State Sci.*, 66 (2017) 44.
14. G. Yuan, Y. Zhao, H. Jin and Z. Bakenov, *Ionics*, 22 (2016) 1819.
15. A. Konarov, D. Gosselink, T.N.L. Doan, Y.G. Zhang, Y. Zhao and P. Chen, *J. Power Sources.*, 259 (2014) 183.
16. G.M. Zhou, S.F. Pei, L. Li, D.W. Wang, S.G. Wang, K. Huang, L.C. Yin, F. Li and H.M. Cheng, *Adv. Mater.*, 26 (2014) 625.
17. X. Zhou, Y. Li, G. Ma, Q. Ma and Z. Lei, *J. Alloy. Comp.*, 685 (2016) 216.
18. C. Wang, X. Wang, Y. Wang, J. Chen, H. Zhou and Y. Huang, *Nano Energ.*, 11 (2015) 678.
19. S. Liu, Y. Li, X. Hong, J. Xu, C. Zheng and K. Xie, *Electrochim. Acta.*, 188 (2016) 516.
20. J. Zhao, S. Pei, W. Ren, L. Gao and H.M. Cheng, *ACS Nano.*, 4 (2010) 5245.
21. H.C. Kang and K.E. Geckeler, *Polymer*, 41 (2000) 6931.
22. Y. Zhang, Z. Bakenov, Y. Zhao, A. Konarov, T.N.L. Doan, M. Malik and P. Chen, *J. Power*

Sources, 208 (2012) 1.
23. M.A. Pimenta, G. Dresselhaus, M.S. Dresselhaus, L.G. Cancado, A. Jorio and R. Saito, *Phys. Chem. Chem. Phys.*, 9 (2007) 1276.
24. J. Schuster, G. He, B. Mandlmeier, T. Yim, K.T. Lee, T. Bein and L.F. Nazar, *Angew. Chem. Int. Ed.*, 51 (2012) 3591.
25. Y. Yang, G. Yu, J.J. Cha, H. Wu, M. Vosgueritchian, Y. Yao, Z. Bao and Y. Cui, *ACS Nano.*, 5 (2011) 9187.
26. G. Yuan, G. Wang, H. Wang and J. Bai, *J. Nanopart. Res.*, 17 (2015) 36.
27. J. Kim, D.J. Lee, H.G. Jung, Y.K. Sun, J. Hassoun and B. Scrosati, *Adv. Funct. Mater.*, 23 (2013) 1076.
28. D. Aurbach, *J. Power Sources*, 119 (2003) 497.
29. X. Liang, Y. Liu, Z. Wen, L. Huang, X. Wang and H. Zhang, *J. Power Sources*, 196 (2011) 6951.
30. Z. Li, J. Zhang and X.W. Lou, *Angew. Chem. Int. Ed.,* 54 (2015) 12886.
31. G. Yuan and J. Xiang, 19 (2013) 1449.
32. H. Peng, J**.** Huang, M**.** Zhao, Q**.** Zhang, X**.** Cheng, X**.** Liu, W**.** Qian and F**.** Wei**,** *Adv. Funct. Mater.***,** 24 **(**2014**)** 2772.
33. J. Xu, W. Zhang, Y. Chen, H. fan, D. Su and G. Wang, *J. Mater. Chem. A*, 2018, DOI: 10.1039/C7TA10272K.
34. Q. Pang, D. Kundu, M. Cuisinier and L.F. Nazar, *Nat. Commun.*, 5 (2014) 4759.
35. X. Wu, Y. D, P. Wang, L. Fan, J. Cheng, M. Wang, Y. Qiu, B. Guan, He. Wu, N. Zhang and K. Sun, *J. Mater. Chem. A*, 5 (2017) 25187.
36. G. Yuan, H. Jin, Y. Jin and L. Wu, *J. Solid State Electrochem.*, 22 (2018) 693.